Applied Chemistry Today **18(69)** (2023) 113-136

Semnan University

Applied Chemistry Today

Journal homepage: https://chemistry.semnan.ac.ir/

ISSN: 2981-2437

Research Article

New pyrazolone-based Schiff base Cu(II) complexes: Synthesis, spectra, theoretical calculation and protein binding

Sakineh Parvarinezhad, Mehdi Salehi*

Department of Chemistry, Faculty of Science, Semnan University, Semnan, Iran

PAPER INFO

Article history:
Received: 29/Aug/2022
Revised: 08/Nov/2022
Accepted: 15/Nov/2022

Keywords:
Pyrazolone; Schiff base; Cu (II) complex; computational chemistry; docking study.

ABSTRACT

In this study, five Schiff base ligands of the NO type were synthesized through the condensation of 4-aminoantipyrine with different aldehydes. These aldehydes include 3,5-dibromo-2-hydroxybenzaldehyde **(HL^1)**, 3,5-dichloro-2-hydroxybenzaldehyde **(HL^2)**, 3,5-diiodo-2-hydroxybenzaldehyde **(HL^3)**, 3-ethoxy-2- hydroxybenzaldehyde **(HL^4)** and 2-hydroxy-1- naphtaldehyde **(HL^5)**. Copper(II) complexes were then prepared using these ligands. The synthesized complexes were characterized using various spectroscopic techniques such as spectrometry, IR, UV-Vis, and electrochemical (CV) methods. Elemental analysis was also performed to determine the elemental composition of the complexes. To gain further insight into the structural features and properties of the complexes, computational methods were employed. The optimization of the complex structures was carried out using Gaussian 09 software with the B3LYP 6-311G basis set. This allowed for the determination of important physical characteristics of the complexes. Frequency calculations were performed to obtain vibrational frequencies, while UV-Vis calculations were carried out to explain the electronic absorption spectra of the complexes. The experimental results obtained from the various spectroscopic techniques were compared with the theoretical results obtained from the computational studies. Theoretical exploration of the frontier molecular orbitals and energy gaps of the complexes provided insight into their electronic structures and stability. Furthermore, molecular docking studies were conducted to investigate the binding affinity of the tested complexes towards STAT3. The Protein Data Bank (PDB) entry 1bg1 was used as the target protein. By analyzing the docking results and summarizing the interactions during the binding process, the complexes exhibited potential effectiveness as inhibitors against colon cancer. Metal complexes (**1-5**) showed that they may be used as new drug candidates for colon cancer. The molecular binding of copper complexes compared to **Crizotinib**, and **niclosamide** (as a drug) showed that they have a better performance and are completely placed in the active site of the receptor. So, the present study gives a new insight for in vivo investigation of the complexes.

DOI: https://doi.org/10.22075/CHEM.2024.32451.2227

* **.Corresponding author:** Professor of Inorganic Chemistry, Department of Chemistry, Faculty of Science, Semnan University, Semnan, Iran. *E-mail address: msalehi@semnan.ac.ir*

How to cite this article: Parvarinezhad, S., & Salehi, M. (2023). New pyrazolone-based Schiff base Cu(II) complexes: Synthesis, spectra, theoretical calculation and protein binding. *Applied Chemistry Today*, **18(69)**, 113-136. (in Persian)

1. Introduction

Pyrazolone compounds have a five-membered heterocyclic ring structure with two adjacent nitrogen atoms. Pyrazolone compounds are used in natural products, and as biologically active substances in drug preparation [1, 2]. Antipyrine is prescribed as a medicine to reduce pain and fever, and this compound is considered as the first product of pyrazole derivatives [3-5]. The special properties of pyrazole compounds, such as versatility and bioactivity, have attracted the attention of many chemists. Hence, they were encouraged to investigate the biological effects of such compounds by synthesizing new compounds. Also, the coordination ability of pyrazole compounds has been the subject of extensive research for the preparation and investigation of Schiff bases and transition metal complexes [6-10]. Some pyrazolone ligands have interesting properties. These compounds are considered chelating agents to stabilize metal ions with different oxidation states [11-14]. Transition metal complexes, in addition to being biologically active, have wide applications such as polymerization, oxidation, dyes and pigments, catalysis, etc. [15-20]. Dangerous tumors have attracted everyone's attention and cause cancer [21]. Therefore, a lot of study and research has been done in this field, such as making changes in cancer cells or increasing the resistance of cells to drugs [22, 23]. Recently, due to the various medicinal and analytical applications of heterocyclic compounds and also their significant interaction with DNA bases, researchers have focused on the synthesis of transition metal complexes derived from such ligands [24, 25]. In addition, copper (II) ion as an important catalytic element can provide an effective biological role in living systems [26]. In recent studies, there are many reports on the vital and anticancer activity of copper complexes derived from benzimidazole, thiosimicarbazone, and Pyrazole ligands have been presented [27]. By comparing these compounds, it was found that the complexes of pyrazole ligand derivatives are the strongest anti-tumor agents, and this compound can be a suitable candidate to be compared with cisplatin drugs [28-30]. In addition, other copper (II) complexes of pyrazole derivatives showed effective and excellent analytical and pharmaceutical applications. Through the investigations and studies in the Crystal Structure Database (CSD), it can be understood that there are limited reports on the crystal structures of Schiff base complexes of pyrazolone derivatives [31-40]. Continuing our work and based on the results of previous reports [40], we decided to synthesize new copper complexes from pyrazolone derivatives (**Scheme. 1**). The copper complexes were elucidated by spectroscopic techniques to determine the accuracy of their synthesis. Intensive structural analysis was performed for the new complexes to obtain diverse physical properties. To simulate the X-ray single crystal analysis, which we failed to provide, calculations such as UV-Vis and frequency spectroscopy were performed using the DFT computational chemistry method using Gaussian 09 software. In the following, the obtained results were compared with the experimental results for the correctness of the synthesis. In addition, molecular docking was used to investigate the interaction behavior of the synthesized compounds against cancer cell proteins to evaluate its inhibitory effect against infected cells after treatment with cytotoxic drugs such as Cu(II) complexes.

2. Experimental

2.1. Methods

All the chemicals' materials and solvents utilized in this research were purchased from Merck and Sigma & Aldrich. The FT-IR was gained as a KBr plate by a Shimadzu 8400S FTIR instrument in the area of 4000-400 cm-1. UV–Vis spectra were established

on a Shimadzu UV-1650 PC spectrophotometer in DMSO solution. Elemental analyses were done on an Elmentar Vario CHNSO and PerkiElmerer device. Electrochemical behavior (CV) was performed on a Metrohm 757 VA Computrace instrument at room temperature in DMSO solution.

2.2.2. Synthesis of Cu(II)-pyrazolone complexes

Each Cu(II) complex of (0.25 mmol, 0.04 g) $Cu(NO_3)_2.3H_2O$ salt was prepared, which was dissolved in 10 ml of ethanol and then added to the ethanolic solution of pyrazolone derivatives ligand (**HL^{1-5}**) (0.25 mmol). Each reaction mixture was refluxed for 4 hours at a temperature of 85°C. The result of the reflux process was a green-coloured solution. This solution was kept at room temperature until after 6 days and the slow evaporation of the solvent, dark green crystals appeared and then it was filtered using a vacuum pump, washed by EtOH solvent. The obtained crystals were not suitable for crystallographic analysis, they were identified using elemental analysis, infrared spectroscopy, and electron transmissions. notification; The synthesis process of copper complexes was shown schematically in **Scheme 1** for ease of understanding.

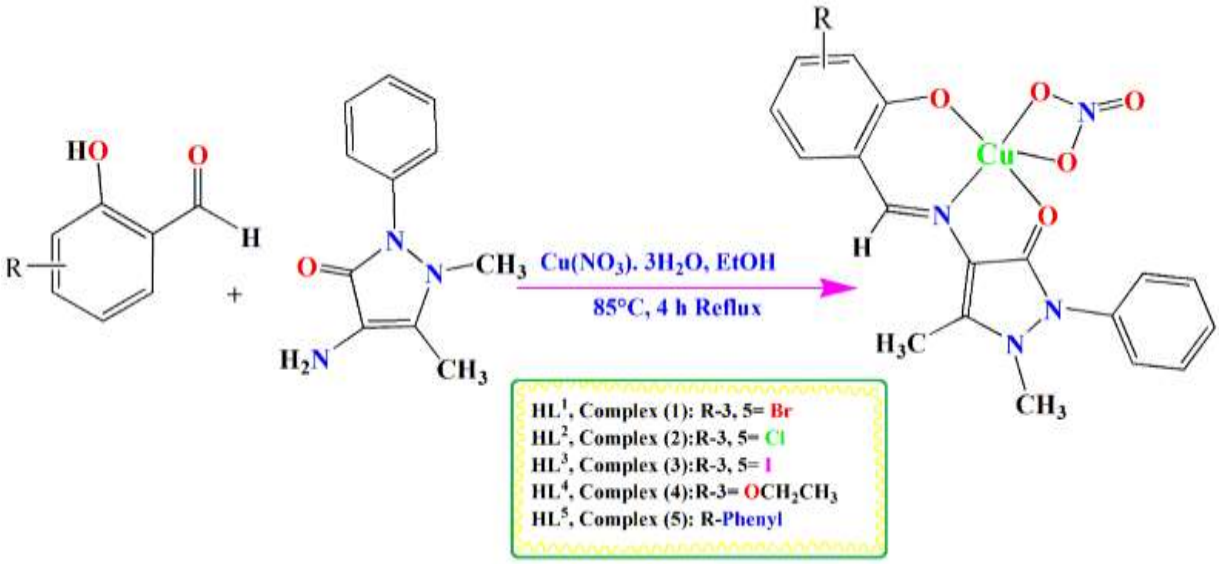

Scheme 1. Synthetic procedure for the preparation of the Cu(II) complexes pyrazolone-based Schiff bases.

Complex (1): Green crystals. Yield: 68%. Mol.Wt: 589.68 g/mol. Anal. Calc. for $C_{18}H_{14}Br_2CuN_4O_5$: C, 36.66; H, 2.39; N:9.50 %. Found: C, 36.20; H; 2.28; N, 9.23%. FT-IR: ν_{max} cm^{-1} (KBr): 3056, 2933 2800(υ_{C-H}), 1612 ($\upsilon_{C=O}$)$_{pyrazolone}$, 1600 (υC=N), 1224, 1294(υ_{C-O}), 692 (υ_{Cu-O}), 561 (υ_{Cu-N}). UV–Vis: λ_{max} (nm) (ε, M^{-1} cm^{-1}) (DMSO): 293 (190000), 339 (63000), 388 (74000), 437(42000), 630 (190).

Complex (2): Green crystals. Yield: 88%. Mol.Wt: 500.78 g/mol. Anal. Calc. for $C_{18}H_{14}Cl_2CuN_4O_5$: C, 43.17; H, 2.82; N, 11.19%. Found: C, 42.98; H; 2.58; N, 11.02%. FT-IR: ν_{max} cm^{-1} (KBr): 3056, 2933 2800(υ_{C-H}), 1660 ($\upsilon_{C=O}$)pyrazolone, 1609 ($\upsilon_{C=N}$), 1296(υ_{C-O}), 692 (υ_{Cu-O}), 563 (υ_{Cu-N}). UV–Vis: λ_{max} (nm) (ε, M^{-1} cm^{-1}) (DMSO): 293 (170000), 340 (61000), 375 (88000), 438 (22000), 578 (1000).

Complex (3): Green crystals. Yield: 68%. Mol.Wt: 683.68 g/mol. Anal. Calc. for $C_{18}H_{14}I_2CuN_4O_5$: C, 31.62; H, 2.06; N, 8.19%. Found: C, 31.34; H; 1.98; N, 8.06%. FT-IR: ν_{max} cm^{-1} (KBr): 3048, 2976 2820(υ_{C-H}), 1646 ($\upsilon_{C=O}$)pyrazolone, 1586 ($\upsilon_{C=N}$), 1296(υ_{C-O}), 626-690 (υ_{Cu-O}), 574 (υ_{Cu-N}). UV–Vis: λ_{max} (nm) (ε, M^{-1} cm^{-1}) (DMSO): 292 (180000), 293 (40000), 346 (58000), 390 (62000), 443(19000), 650 (268).

Complex (4): Green crystals. Yield: 68%. Mol.Wt: 475.94 g/mol. Anal. Calc. for $C_{20}H_{20}CuN_4O_5$: C, 50.47; H, 4.24; N, 11.77%. Found: C, 50.30; H; 4.11; N, 11.43%. FT-IR: ν_{max} cm^{-1} (KBr): 3061, 2945 2810(υ_{C-H}), 1640 ($\upsilon_{C=O}$)pyrazolone, 1598 ($\upsilon_{C=N}$), 1296(υ_{C-O}), 657 (υ_{Cu-O}), 543 (υ_{Cu-N}). UV–Vis: λ_{max} (nm) (ε, M^{-1} cm^{-1}) (DMSO): 291 (160000), 333 (36000), 350 (34000), 411 (29000), 435(25000), 650 (280).

Complex (5): Green crystals. Yield: 62%. Mol.Wt: 481.95 g/mol. Anal. Calc. for $C_{22}H_{18}CuN_4O_5$: C, 54.83; H, 3.76; N, 11.63%. Found: C, 54.45; H; 3.48; N, 11.39%. FT-IR: ν_{max} cm^{-1} (KBr): 3210, 3028, 3025, 2922, 2848 and 2752 (υ_{C-H}), 1601 ($\upsilon_{C=O}$)pyrazolone, 1581 ($\upsilon_{C=N}$), 1294 (υ_{C-O}), 692 (υ_{Cu-O}), 551-588 (υ_{Cu-N}). UV–Vis: λ_{max} (nm) (ε, M^{-1} cm^{-1}) (DMSO): 285 (34000), 296(49000), 331 (38000), 346 (36000), 404(39000), 431(61000), 451(65000), 686 (110).

2. 3. Electrochemical studies, cyclic voltagram (CV)

Using cyclic voltammetry (CV), the potential values of oxidation and reduction regions as well as the electrochemical behavior of the synthesized copper complexes were studied. Therefore, silver wire reference electrodes, platinum auxiliary electrodes, and glassy carbon work electrodes are needed to perform electrochemical analysis. Also, to perform this analysis, an electrolyte solution is needed, and tetrabutylammonium hexafluorophosphate salt with a concentration of 10^{-1} M in dimethyl sulfoxide solution was used to prepare the electrolyte solution. The cyclic voltammogram process was carried out at a temperature of 25 °C and under argon gas conditions to remove oxygen from the reaction medium and with a scanning speed of 100 mV/s. Also, after each scan, the working electrode was polished with alumina powder to remove any contamination, and in this analysis, all the potentials of the oxidation and reduction regions were calibrated using ferrocene as an internal standard ($E_{1/2}$ = 0.42 V) [45, 46]. The electrochemical behavior information along with oxidation and reduction values with cyclic voltagram diagrams of the prepared complexes are presented in the third part of this study.

2.4. Theoretical approach

2.4.1. Optimization process

The structure of all copper complexes were optimized using standard software Gaussian 09 [47]. Frequency calculations and electron transitions were calculated with the DFT/B3LYP method in order to minimize the energy in the default solvent of dimethyl sulfoxide under a 6-311G basis set. The structure of target complexes and calculation files (out, chk, etc.) were collected. To compare the experimental results with the computational results to determine the correctness of the structure of the complexes as well as to extract other physical properties, the computational files were opened using the Gauss View program, and viewed as a numbered plot on the Gauss View screen [48]. In the following, using the mentioned equations [49, 50] and using the HOMO and LUMO energy gap, more parameters were investigated:

$$E_{GAP} = E_{LUMO} - E_{HOMO} \quad (1)$$

$$\chi = -1/2(E_{LUMO} + E_{HOMO}) \quad (2)$$

$$\mu = -\chi \quad (3)$$

$$\eta = 1/2(E_{LUMO} - E_{HOMO}) \quad (4)$$

$$S = \frac{1}{2\eta} \quad (5)$$

Also, using AIM2000 software with the help of the theory of atoms in molecules (QTAIM), topological properties at critical points were evaluated [51]. MEP maps for all copper complexes were created on the cubic surface through chk and fch files. Some features using red, blue, and green colours created on the maps indicate the nucleophilic, electrophilic, and zero potential regions, which we discuss more in the results and discussion section.

2.4.2. Molecular docking method

In silico study as computational approaches could be used as receptor-based drug design for new anticancer drugs [52-55]. In this work, the protein structure of TRANSCRIPTION FACTOR STAT3B/DNA COMPLEX (1bg1: https://www.rcsb.org/structure/1bg1) was prepared as PDB and applied to predict the binding pose of the compound in STAT3 SH2-binding site by using the software Molegro Virtual Docker. To interact inside receptors, "detect cavities" were selected in 5 parts, then selected Internal ES, Internal HBond and SP2, and SP2 Torsions as well as Fter docking: Energy Minimization. The output was saved as MOL2. The results were investigated by Molegro Molecular Viewer [52-55].

3. Results and discussion

3.1. Synthesis

Copper complexes synthesized from pyrazolone derivatives with a molar ratio of 1Cu: 1HL were proposed. The structure of the complexes derived from the pyrazolone ligand based on we past studies [40] emerged with a simple structure that allows the coordination of a ligand molecule and a metallic copper salt nitrate group without steric hindrance. Dark green colours appeared in the complexes due to d-d transitions and the high effect of charge transfer ،caused this colour change to be observed compared to the yellow pyrazolone ligands, confirming the correctness of the complex synthesis. Characterization of synthesized copper complexes was done using elemental analysis techniques, FT-IR, and UV-Vis spectroscopy. In addition, by using DFT calculations, the molecular structure of the complexes was optimized and confirmed. To predict and determine the correctness of the structures of the synthesized complexes, calculations such as vibration frequency and electron transfer were performed and with the help of the obtained calculation results, they were compared with the experimental results. Furthermore, the molecular simulation was used to investigate the interaction behavior of the synthesized compounds against cancer cell proteins to evaluate their inhibitory effect against infected cells after treatment with cytotoxic drugs.

3.2. FT-IR spectra of the ligands (HL^{1-5}) and complexes (1-5)

By examining the FT-IR spectrum in the range of 4000-400 cm^{-1} (**Figs. S1-5**) for the synthesized ligands and Cu(II) complexes, more significant vibrational bands were extracted. **Table 1** is a summary of the vibration bands listed. Vibrations υ(C=O), υ(C=N), the vibrational bands appearing in the ligands of pyrazolone derivatives compared to the FT-IR spectra of the synthesized Cu (II) complexes, a visible change was recorded towards the lower/higher wave number. These regions can indicate the participation of these groups in the coordination through the binding mode of neutral bidentate. Also, the presence of nitrate anion in coordinated Cu (II) complexes appeared through the bidentate state. During complexation, the υ(M-O) and υ(M-N) bands were assigned in the lower wavenumber region in the spectra of the complexes, which proves the correct coordination of copper [56]. The vibrational spectrum of pyrazolone ligands has shown a prominent vibrational band in the region of 1251 to 1269 cm^{-1}, which is specific to the phenolic/naphthol C-O stretching vibration. During complexation, this region has emerged as a stretching band with a higher frequency of 1294-1296 cm^{-1}, which also confirms the coordination of the phenolic/naphtholic oxygen of the ligand to the copper metal [38-40, 57-61]. In addition, the nonappearance of a phenolic/naphtholic O-H stretching vibration band at about 3400-3600 cm^{-1} in the complexes also confirms the deprotonation of the pyrazolone ligands. The electronic structures of the studied copper complex were first optimized by

the Gauss 09 program in the gas phase, at the level of theory (B3LYP/6-311G), and the optimized structure of the complexes in **Fig. 1** is shown. The vibrational frequencies of the studied copper complexes were calculated using the DFT/B3LYP method with the 6-311 G basis set. The theoretical and experimental results of copper complexes are shown in **Table 1**. According to the results collected in **Table 1**, the agreement between experimental frequencies and computational chemistry is generally very good. The C-H stretching vibrational mode is observed experimentally in the region of 2700-3200 cm^{-1}, while it was calculated using computational chemistry to be in the region of 3011-3231 cm^{-1}, which is shifted to higher wavenumbers than the experimental values. The region of 1581-1618 cm^{-1} can be attributed to the proton transfer of Schiff bases and stretching vibration of azomethine (C=N) bond, while it was calculated in the region of 1601-1644 cm^{-1} using B3LYP. The observed bands at 626- 692 cm^{-1} and 543-588 cm^{-1} are related to the stretching vibrations of metal-oxygen and metal-nitrogen, which have appeared in the regions of 605-697 cm^{-1} and 496-526 cm^{-1}, respectively, using the calculation method. In addition, the regions of 1251-1296 cm^{-1} confirm the presence of a phenol group in the compound. The same bands in the regions of 1271-1369 cm^{-1} by the B3LYP method show good agreement with FT-IR bands. The above results are in good agreement with similar Schiff base compounds.

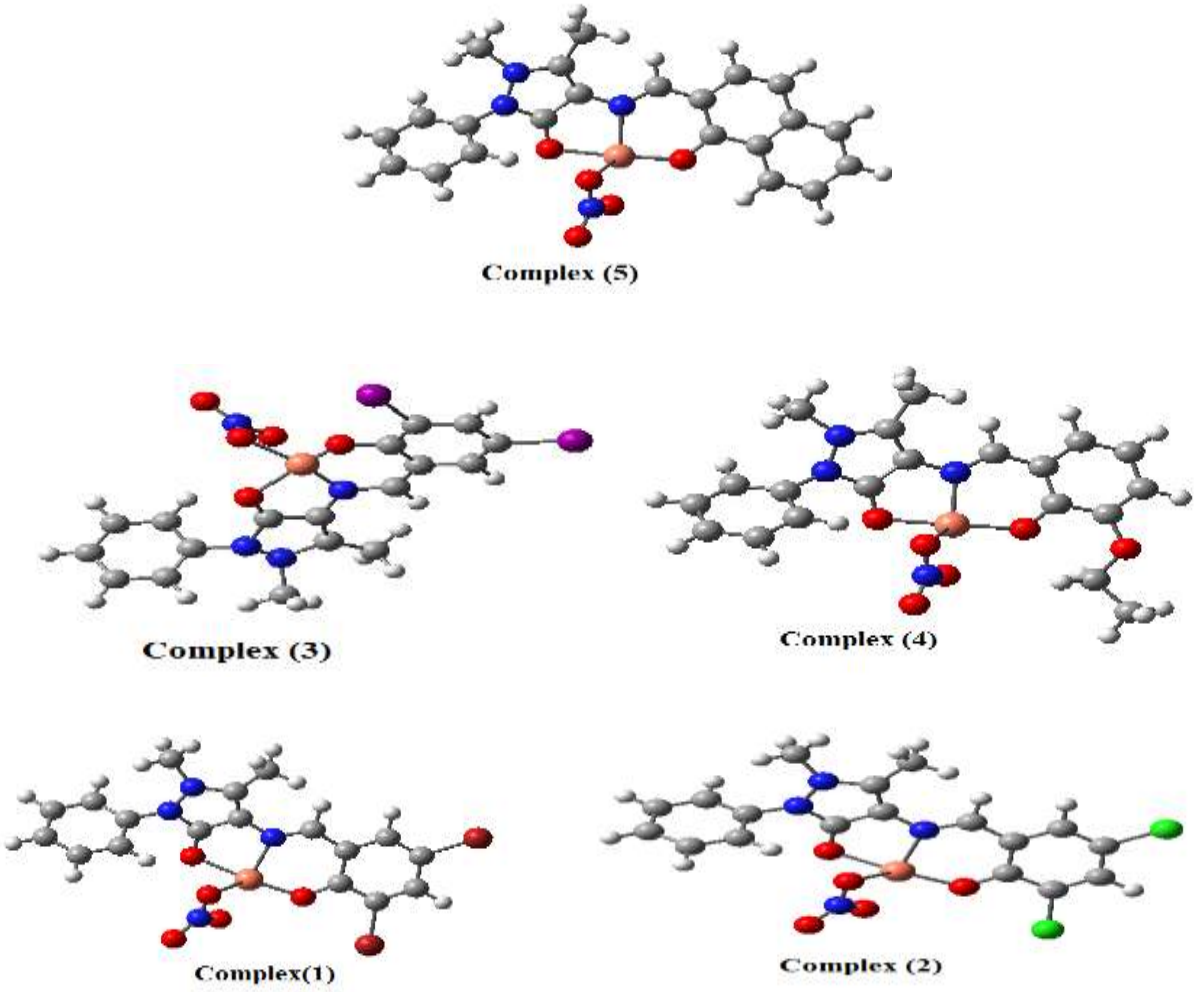

Figs. 1 optimized molecular structures of complexes (1-5).

Table 1. Experimental and theoretical properties of pyrazole derivatives ligands and their complexes.

Experimental (cm^{-1})	Theoretical	Tentative assignment
	HL^1	
1622	-	$\upsilon_{(C=O)}$
1580	-	$\upsilon_{(C=N)}$
3450	-	$\upsilon_{(O-H)}$
2920-3080	-	$\upsilon_{(C-H)}$
1272	-	$\upsilon_{(C-O)}$
	Complex (1)	
1612	1662	$\upsilon_{(C=O)}$
1600	1643	$\upsilon_{(C=N)}$
-	-	$\upsilon_{(O-H)}$
2800-3056	3022-3219	$\upsilon_{(C-H)}$
1294	1311-1343	$\upsilon_{(C-O)}$
692	630-697	$\upsilon_{(M-O)}$
561	500	$\upsilon_{(M-N)}$
	HL^2	
1664	-	$\upsilon_{(C=O)}$
1618	-	$\upsilon_{(C=N)}$
3419	-	$\upsilon_{(O-H)}$
2700-3000	-	$\upsilon_{(C-H)}$
1276	-	$\upsilon_{(C-O)}$
	Complex (2)	
1660	1658	$\upsilon_{(C=O)}$
1609	1643	$\upsilon_{(C=N)}$
-	-	$\upsilon_{(O-H)}$
2800-3056	3022-3224	$\upsilon_{(C-H)}$
1296	1320-1342	$\upsilon_{(C-O)}$
692	613-653	$\upsilon_{(M-O)}$
563	504	$\upsilon_{(M-N)}$
	HL^3	
1662	-	$\upsilon_{(C=O)}$
1593	-	$\upsilon_{(C=N)}$
3434	-	$\upsilon_{(O-H)}$
2700-3000	-	$\upsilon_{(C-H)}$
1272	-	$\upsilon_{(C-O)}$
	Complex (3)	
1646	1661	$\upsilon_{(C=O)}$
1586	1601-1630	$\upsilon_{(C=N)}$
-	-	$\upsilon_{(O-H)}$
2800-3056	3052-3231	$\upsilon_{(C-H)}$
1296	1331-1368	$\upsilon_{(C-O)}$
626-690	605-676	$\upsilon_{(M-O)}$
574	496	$\upsilon_{(M-N)}$
	HL^4	
1649	-	$\upsilon_{(C=O)}$
1585	-	$\upsilon_{(C=N)}$
3400-3600	-	$\upsilon_{(O-H)}$
2748-2977	-	$\upsilon_{(C-H)}$
1251-1272	-	$\upsilon_{(C-O)}$
	Complex (4)	
1640	1664	$\upsilon_{(C=O)}$
1598	1609-1644	$\upsilon_{(C=N)}$
-	-	$\upsilon_{(O-H)}$
2800-3000	3014-3207	$\upsilon_{(C-H)}$
1296	1271-1300	$\upsilon_{(C-O)}$
657	621-693	$\upsilon_{(M-O)}$
543	499-526	$\upsilon_{(M-N)}$
	HL^5	
1652	-	$\upsilon_{(C=O)}$
1591	-	$\upsilon_{(C=N)}$
3400-3600	-	$\upsilon_{(O-H)}$
2700-3200	-	$\upsilon_{(C-H)}$
1269	-	$\upsilon_{(C-O)}$
	Complex (5)	
1602	1660	$\upsilon_{(C=O)}$

1581	1609-1634	$\upsilon_{(C=N)}$
-	-	$\upsilon_{(O-H)}$
2800-3025	3011-3214	$\upsilon_{(C-H)}$
1296	1317-1369	$\upsilon_{(C-O)}$
692	607-654	$\upsilon_{(M-O)}$
551-588	480-532	$\upsilon_{(M-N)}$

3.3. Spectroscopic characterizations to be UV-Vis of the ligands (HL^{1-5}) and complexes (1-5)

The spectrum of electron transitions of each scanned set in the range of 200-800 nm is presented in **Fig. S6-10**. In the spectrum of the copper complex, transitions are observed due to the splitting of the d shell of the metal ion, as well as intra-ligand transitions. Using this technique, it is possible to determine the degree of fission corresponding to a given geometry. In **Table 2**, transitions such as intra-ligand transitions, MLCT, and d → d transitions have been extracted. According to the results shown in **Table 2**, it can be understood that transitions such as $n\rightarrow\pi^*$, and $\pi\rightarrow\pi^*$ in coordinating ligands have been observed in deep ultraviolet regions [62]. The UV-Vis spectrum of the synthesized copper complexes is close to the square planar geometry and is distorted due to John Teller's distortion [63]. This proposed geometry is due to the band observed in each spectrum, in the 578-690 nm region, which is attributed to d → d transitions [63]. These results confirm the correctness of the complex synthesis. According to the figures of the electron transfer spectrum of the ligand, the peak observed in the region of 210-243 nm is due to the $\pi \rightarrow \pi^*$ transition of the phenyl rings and the absorption band (λ_{max}) in the region of 260-329 and 325-435 nm is to the intramolecular charge transfer band $\pi \rightarrow \pi^*$ and $n \rightarrow \pi^*$ of the azomethine group C = N is relevant. Also, these values are similar to those found in related Schiff base compounds [38-40, 64, 65]. In the spectrum of studied copper complexes, these areas appear in higher amounts, and their information is presented in **Table 2**. The electronic absorption spectrum of the complexes was calculated by the DFT method based on the optimized structure at the B3LYP/6-311 G level in the gas phase. The calculation results were compared with the experimental absorption spectrum data in **Table 2**. For computational chemistry, the theoretical absorption bands related to the electron transfer of the azomethine group at 395-434 nm (for **complex (1)**), 453 nm (for **complex (2)**), 381-467 nm (for complex (3)) nm, 411-461 nm (for **complex (4)**) and 436-460 nm (for **complex (5)**) regions were predicted with transfer energies of 3.1327-2.8520, 2.7343, 3.8124-2.7450, 3.0096-2.6838 and 2.8400-2.6919 eV, respectively. In addition, the experimental spectra of metal-to-ligand charge transfer (MLCT) complexes with wavelengths in the regions of 437 nm (for **complex (1)**), 438 nm (for **complex (2)**), 443 nm (for **complex (3)**), 411-435 nm (for **complex (4)**) and 429-452 nm (for **complex (5)**) were observed to have a square planar geometry, the result of computational chemistry with higher values in the mentioned table has been provided. Also, the d-d transition for each of the copper complexes, the regions obtained using computational chemistry at 612-667nm (for **complex (1)**), 570-658 nm (for **complex (2)**), 671-715 nm (for **complex (3)**), 595-650 nm (for **complex (4)**) and 596-757 nm (for **complex (5)**) with transfer energies of 2.0251-1.8567, 2.1748-1.4449, 1.8456- 1.7325, 2.0803-1.9072 and 2.0771-1.6364 eV is observed. According to the obtained results, it can be easily concluded that they are consistent with the experimental absorption. **Complex (2)** shows a higher energy gap and higher chemical hardness compared to other copper complexes, which result will be explained in the interpretation section of the frontier molecular orbital analysis (FMOs).

Table 2. Experimental and theoretical UV-Vis spectra results of pyrazole derivatives ligands and their complexes.

Experimental (nm)	Theoretical (nm)	Transitions assignment
HL^1		
236	-	$(\pi\rightarrow\pi^*)_{\text{aromatic ring}}$
290	-	$(\pi\rightarrow\pi^*)_{C=N}$
356	-	$(n\rightarrow\pi^*)_{C=N}$
Complex (1)		
293	378-384	$(\pi\rightarrow\pi^*)_{\text{aromatic ring}}$
339-388	395-434	$(\pi\rightarrow\pi^*)_{C=N}$
437	509	MLCT
630	612-667	d → d
HL^2		
228-232	-	$(\pi\rightarrow\pi^*)_{\text{aromatic ring}}$
273-292	-	$(\pi\rightarrow\pi^*)_{C=N}$
378-429	-	$(n\rightarrow\pi^*)_{C=N}$
Complex (2)		
293	374-398	$(\pi\rightarrow\pi^*)_{\text{aromatic ring}}$
340-375	453	$(\pi\rightarrow\pi^*)_{C=N}$
438	544-555	MLCT
578	570-658	d → d
HL^3		
241	-	$(\pi\rightarrow\pi^*)_{\text{aromatic ring}}$
298-329	-	$(\pi\rightarrow\pi^*)_{C=N}$
380-435	-	$(n\rightarrow\pi^*)_{C=N}$
Complex (3)		
292-293	368	$(\pi\rightarrow\pi^*)_{\text{aromatic ring}}$
346-390	381-467	$(\pi\rightarrow\pi^*)_{C=N}$
443	521	MLCT
650	671-715	d → d
HL^4		
210	-	$(\pi\rightarrow\pi^*)_{\text{aromatic ring}}$
228-270	-	$(\pi\rightarrow\pi^*)_{C=N}$
334	-	$(n\rightarrow\pi^*)_{C=N}$
Complex (4)		
291	382	$(\pi\rightarrow\pi^*)_{\text{aromatic ring}}$
333-350	411-461	$(\pi\rightarrow\pi^*)_{C=N}$
411-435	481-547	MLCT
650	595-650	d → d
HL^5		
225-243	-	$(\pi\rightarrow\pi^*)_{\text{aromatic ring}}$
260-290	-	$(\pi\rightarrow\pi^*)_{C=N}$
325-400	-	$(n\rightarrow\pi^*)_{C=N}$
Complex (5)		
285-296	398-424	$(\pi\rightarrow\pi^*)_{\text{aromatic ring}}$
333-347	436-460	$(\pi\rightarrow\pi^*)_{C=N}$
429-452	489-525	MLCT
686	596-757	d → d

3.4. Electrochemistry of the complexes (1-5)

Cyclic voltammetry for the studied copper complexes in DMSO solvent is presented in **Figs. 2**. According to the obtained results, which we will discuss further, the synthesized copper complexes have shown a quasi-reversible behavior. The voltammogram in the cathodic region (Epc) around -0.63, -0.80 to -0.90 V is attributed to the reduction process of $Cu^{(II)}/Cu^{(I)}$. In addition, the anodic voltammogram at -0.49, -0.61 to -0.69 V is related to $Cu^{(I)}/Cu^{(II)}$ oxidation [38-40, 54, 55].

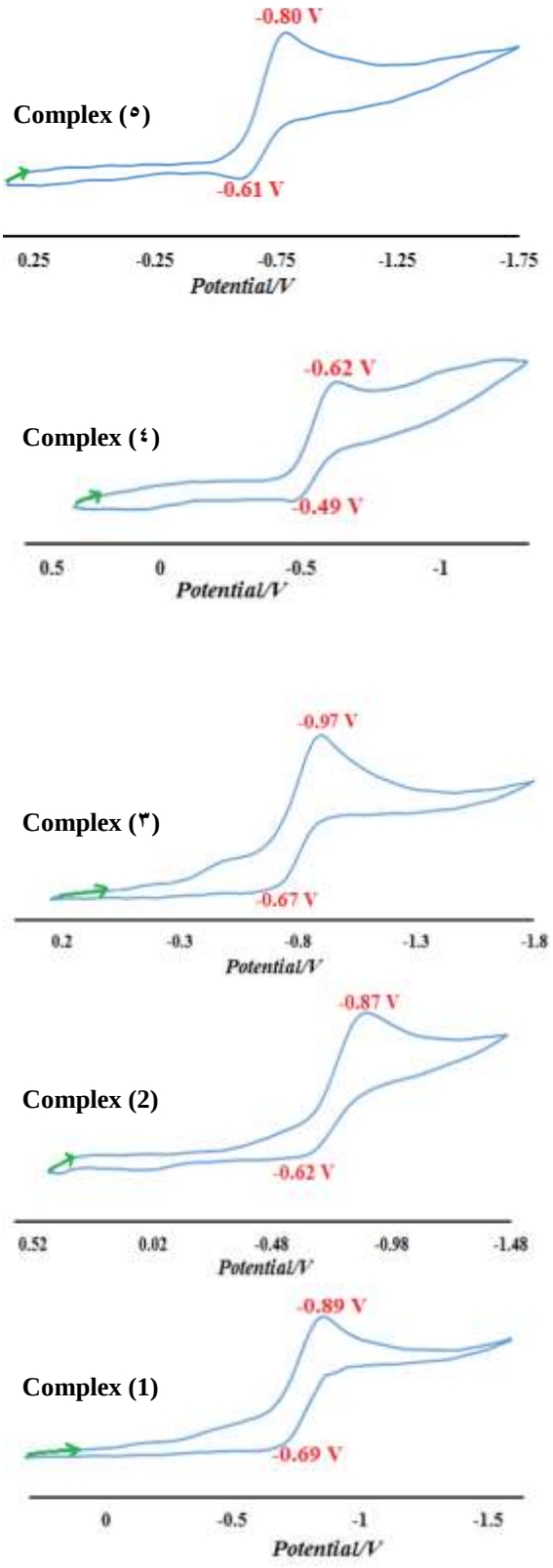

Figs 2. Cyclic voltammogram of 10^{-3} mol L^{-1} solutions of Cu(II) complexes (**1-5**) in DMSO solutions containing 0.1 mol L^{-1} TBAH and scan rate 100 mVs^{-1}.

3.5. Frontier molecular orbital analysis

By studying the frontier molecular orbital (FMO) energy levels of copper complexes, it is concluded that electronic transitions between the highest occupied molecular orbital (HOMO) as an electron donor (electrophilicity) and the lowest unoccupied molecular orbital (LUMO) as an acceptor electron (nucleophilicity) is formed. **Figs. 3** shows the distribution and energy levels of frontier molecular orbitals calculated at the same level of theory for copper complexes. **Table 3** provides information on HOMO and LUMO energy levels of copper complexes. An interesting conclusion can be drawn using the map of frontier molecular orbitals (FMOs). By decreasing the LUMO values, the ability to accept electrons will be higher [51]. In **Table 3**, it is concluded that among the studied complexes, **complex (2)** has the lowest LUMO value compared to others. Also, the energy difference (ΔE) of **complexes (1, 3, 4,** and **5)** is relatively lower than that of **complex (2) (2 > 4 > 3> 1 > 5)**, which shows that copper ion has a stronger potential to accept electrons or donate electrons to It has the title of active center and the biological activity of pyrazolone copper complexes is predicted as **5 > 1> 3> 4 > 2** [66]. Quantum parameters were calculated by using the energy of the orbitals and its information can be seen in **Table 3** [38-40, 51]. The molecule that has the lowest value (ΔE) has more polarity and high chemical reactivity, and this molecule can be selected as a soft molecule (**complex (5)**). By comparing the calculated values of these parameters among copper complexes, **complex (2)** has a more stable structure, due to having a higher HOMO and LUMO energy gap than other complexes, and this complex is shown as a harder molecule. The obtained results can indicate the presence of different interactions or stronger hydrogen bonds in the structure of the **complex (2)** compared to other complexes. In addition, by calculating the negative LUMO and HOMO energy levels, it can be found that all five structures of the complex are stable [67].

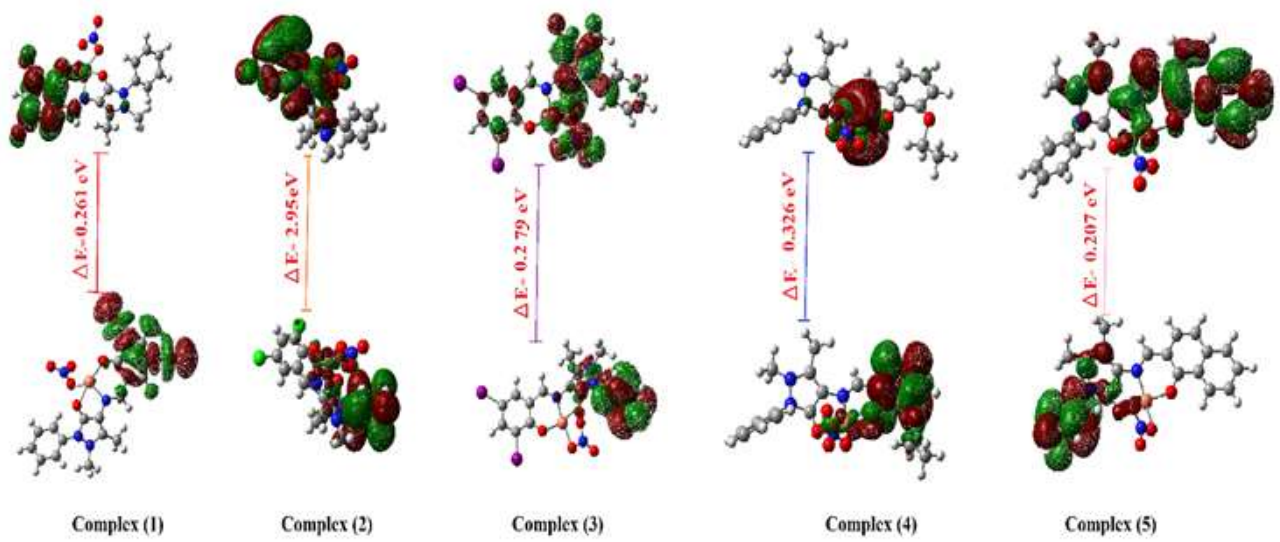

Figs. 3 surface plots of HOMO and LUMO for complexes (**1-5**).

Table 3. Calculated global reactivity descriptors of the complexes (**1-5**) at the B3LYP/6-311G level.

Parameters	Complex (1)	Complex (2)	Complex (3)	Complex (4)	Complex (5)
E_{LUMO} (eV)	-3.688	-0.507	-3.622	-3.411	-3.719
E_{HOMO} (eV)	-3.949	-3.457	-3.901	-3.737	-3.926
$E_{LUMO} - E_{HOMO}$ (eV)	0.261	2.950	0.279	0.326	0.207
$E_{LUMO} + E_{HOMO}$ (eV)	-7.637	-3.964	-7.523	-7.148	-7.645
Electronegativity (χ)	3.818	1.982	3.761	3.574	3.822
Chemical potential (μ)	-3.818	-1.982	-3.761	-3.574	-3.822
Chemical hardness (η)	0.130	1.475	0.139	0.163	0.103
Softness (S)	3.831	0.545	3.584	3.067	4.830

3.3. Molecular electrostatic potential of complexes (1-5)

The purpose of studying the molecular electrostatic potential (MEP) is to investigate the electrostatic interaction between the studied complex molecules [38-40,51]. The MEP of the complexes is shown in **Fig. 4**. The blue region represents the electron-poor part, which is capable of receiving negatively charged ions, and the red region represents the electron-rich and more reactive part. According to all five MEP schemes, it can be understood that oxygen atoms with red colour have a negative electrostatic potential and strong repulsion and are candidates for electrophilic attack. The sites of strong attraction are the greatest possible regions with blue colours, which are observed near the C-H group, and central metal they highly reactive regions for nucleophilic attack. These locations are also presented for hydrogen bonding due to the existence of greatly electronegative atoms C, N, O, Br, Cl, and I.

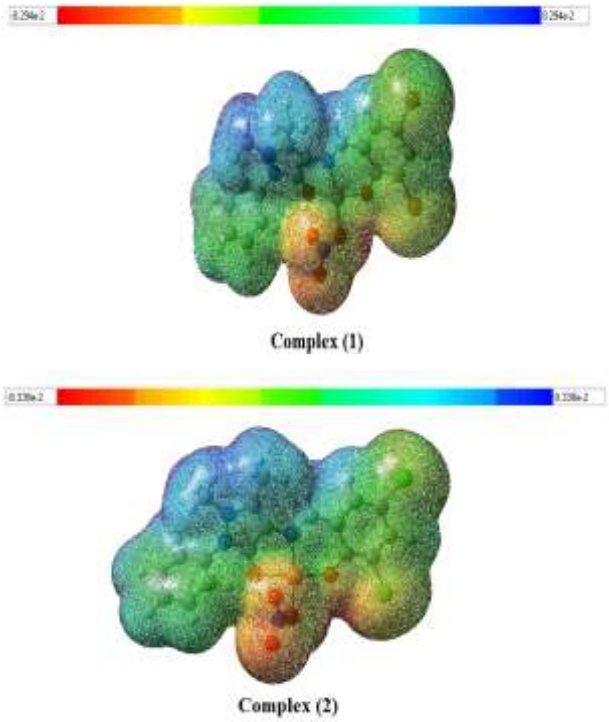

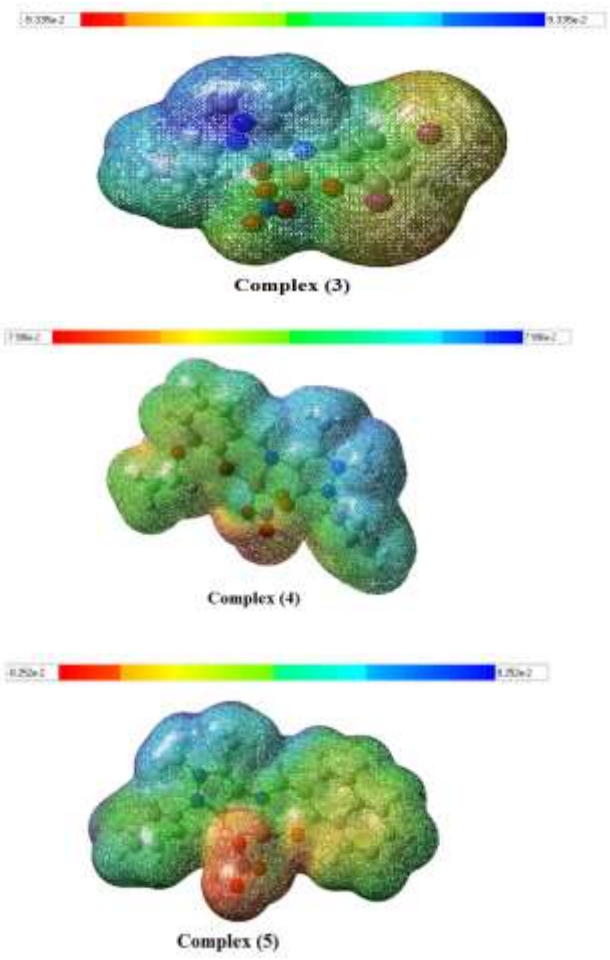

Figs. 3 Molecular electrostatic potential maps (MEP) were calculated at the B3LYP/6311-G level for the studied complexes.

3.4. QTAIM theory of the complexes (1-5)

Molecular interaction in pyrazolone complexes was investigated using the "atom in molecule" theory. This study was conducted to determine the type of bond between M-O/M-N bonds in pyrazolone complexes (**Fig. 5**). In this study, each metal was attached at its strategic positions and optimized using DFT at the same B3LYP/6-311G level of theory. In this theory, the total electron energy density at the bonding critical point (BCP) plays an important role in investigating the interaction involved. According to **Table 4**, low values of electron density $\rho(r)$ and positive values of Laplacian $(\nabla^2\rho(r))$, it can be understood that non-covalent or non-polar interaction is observed in M-O/N bonds. The values of electron density $\rho(r)$ and $(\nabla^2\rho(r))$ from 0.0634 to 0.0958 a.u. and 0.0793 to 0.1395 a.u. are presented in Table 4, respectively. In the following, using a series of energy parameters (**Table 4**), more analysis was done on the charge distribution in M-O/M-N bonds, which confirmed the opposite charge between copper and O/N, and the non-covalent interactions with the ionic character of M-O/N. These parameters describe the interactions using open shell $(\frac{|(V(r))|}{(G(r))} > 2)$ and $H(r) < 0$) and closed shell ($\frac{|(V(r))|}{(G(r))} < 1$) and $H(r) > 0$), describing the type of interactions involved [40, 51, 68, 69]. The results of energy parameters show that the total electron energy density $(H(r))$ for all pyrazolone complexes is calculated with negative values, which can predict polar (open shell) interactions.

On the other hand, the ratio of potential energy density $(V(r))$ to $(G(r))$ is greater than 1 $(\frac{|(V(r))|}{(G(r))} > 1)$, and indicates the intermediate interaction. Negative values of $(\nabla^2\rho(r))$ indicate the tendency of covalent bonds, while positive values indicate non-covalent interactions. Also, positive values of $(\nabla^2\rho(r))$ and $H(r)$ predict electrostatic interaction, and positive values of $(\nabla^2\rho(r))$ and negative $H(r)$ indicate partial covalent interaction. According to the general result obtained from this theory, it is inferred that the bonds (M-O and M-N) in the studied complexes are expected as non-covalent bonds with a noteworthy contribution of ionic nature.

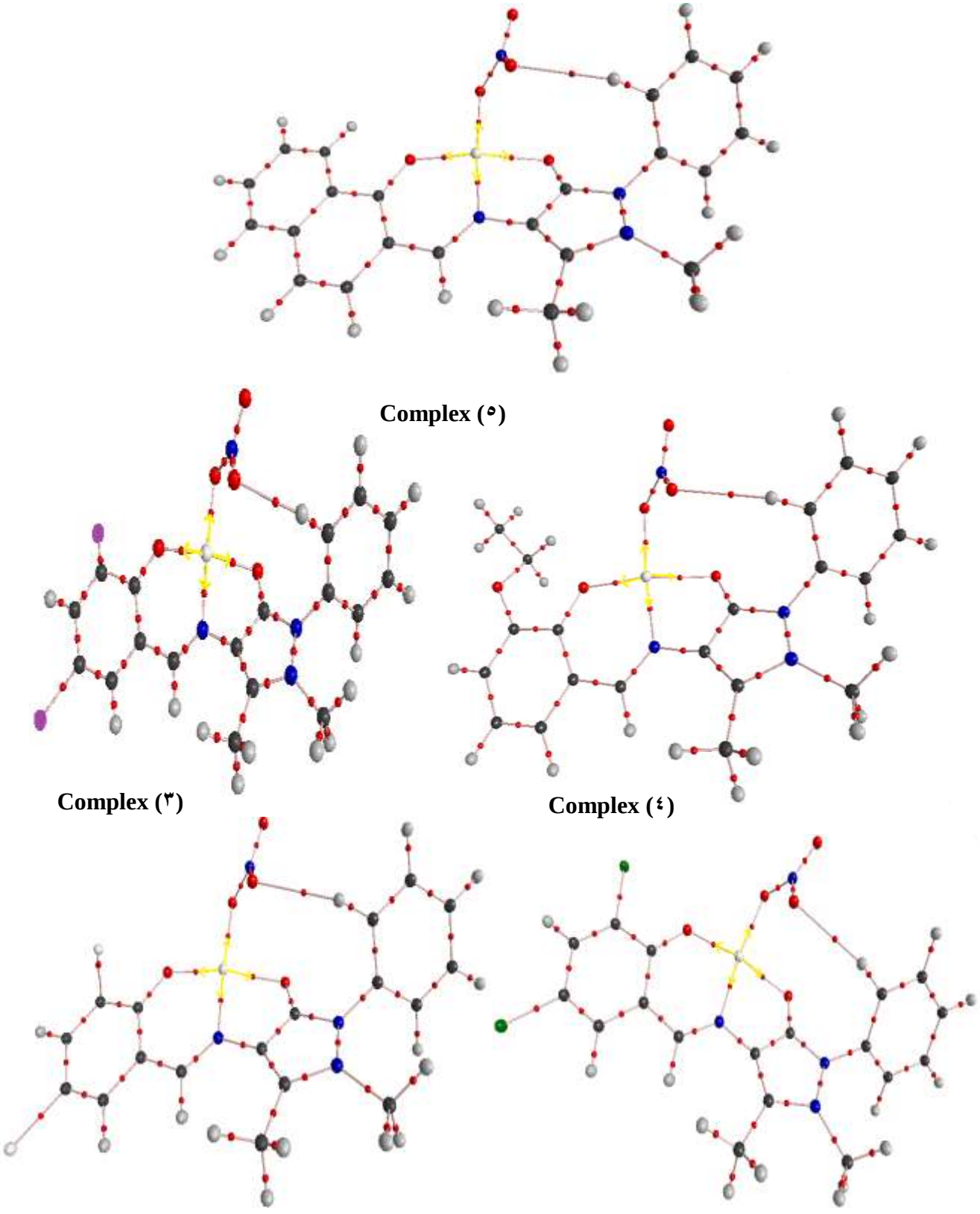

Figs. 5 molecular graphs and distribution of bond critical points for Cu (II) complexes **(1-5)**. Bond critical points (BCP) and bond paths connecting BCP are represented as red spheres and black, respectively. The BCPs at the bond paths connecting atoms around center metal (M…O, and M…N in **Table 4**) are highlighted by yellow arrows, in the figure.

Table 4.Topological properties $\rho(r)$ and $\nabla^2\rho(r)$ (a.u.), kinetic energy density ($G(r)$, in a.u.), -potential energy density ($V(r)$, in a.u.) and total energy density ($H(r)$, in a.u.) for BCP of the studied metal-ligand interactions at the B3LYP/SDD(6-311G) level for the studied complexes.

Intramolecular interaction	$\rho(r)_{BCP}$	$\nabla^2\rho(r)_{BCP}$	$G(r)_{BCP}$	$V(r)_{BCP}$	$H(r)_{BCP}$	$(\frac{\lvert V(r)\rvert}{G(r)})_{BCP}$
Complex (1)						
$(Cu\text{-}N)_{Pyrazolone}$	0.0643	0.0806	0.0859	-0.0912	-0.0052	1.061
$(Cu\text{-}O)_{aldehyde}$	0.0937	0.1377	0.1470	-0.1563	-0.0092	1.063
$(Cu\text{-}N)_{NO3}$	0.0846	0.1133	0.1217	-0.1301	-0.0084	1.069
$(Cu\text{-}N)_{C=N}$	0.0884	0.1024	0.1184	-0.1344	-0.0159	1.135
Complex (2)						
$(Cu\text{-}N)_{Pyrazolone}$	0.0645	0.0808	0.0861	-0.0914	-0.0053	1.061
$(Cu\text{-}O)_{aldehyde}$	0.0933	0.1373	0.1464	-0.1555	-0.0091	1.062
$(Cu\text{-}N)_{NO3}$	0.0848	0.1135	0.1220	-0.1305	-0.0084	1.069
$(Cu\text{-}N)_{C=N}$	0.0879	0.1018	0.1176	-0.1334	-0.0158	1.134
Complex (3)						
$(Cu\text{-}N)_{Pyrazolone}$	0.0661	0.0810	0.0868	-0.0909	-0.0066	1.047
$(Cu\text{-}O)_{aldehyde}$	0.0938	0.1339	0.1468	-0.1563	-0.0090	1.064
$(Cu\text{-}N)_{NO3}$	0.0841	0.1141	0.1282	-0.1369	-0.0086	1.067
$(Cu\text{-}N)_{C=N}$	0.0779	0.0936	0.1056	-0.1472	-0.0171	1.393
Complex (4)						
$(Cu\text{-}N)_{Pyrazolone}$	0.0634	0.0793	0.0845	-0.0896	-0.0051	1.060
$(Cu\text{-}O)_{aldehyde}$	0.0958	0.1395	0.1497	-0.1599	-0.0102	1.068
$(Cu\text{-}N)_{NO3}$	0.0837	0.1129	0.1210	-0.1291	-0.0081	1.066
$(Cu\text{-}N)_{C=N}$	0.0908	0.1048	0.1218	-0.1387	-0.0169	1.138
Complex (5)						
$(Cu\text{-}N)_{Pyrazolone}$	0.0642	0.0806	0.0859	-0.0911	-0.0052	1.060
$(Cu\text{-}O)_{aldehyde}$	0.0934	0.1371	0.1463	-0.1556	-0.0092	1.063
$(Cu\text{-}N)_{NO3}$	0.0837	0.1139	0.1223	-0.1304	-0.0082	1.066
$(Cu\text{-}N)_{C=N}$	0.0917	0.1054	0.1228	-0.1402	-0.0174	1.141

3.5. Molecular docking

Colon cancer is the most dangerous type worldwide. Cancer cell also upregulates other important downstream genes such as Signal transducers and activators of transcription (STAT3), which plays a vital role in cell proliferation, cell survival, metastasis, and angiogenesis in colon cancer. Crizotinib and niclosamide reduce cell viability, cell migration, and invasion in a dose-dependent manner against colon cancer via the interaction with overexpressed STAT3 [70]. Our complexes are similar to two Crizotinib and niclosamide drugs based on benzene and pyrazole rings. So, complexes Cu (II) were carried out for the molecular docking for discovering new drugs and the inhibition tendency of the target cancer protein STAT3 (1bg1). According to the molecular docking results, it is concluded that all five complexes can effectively interact with the molecular target cancer protein STAT3 (1bg1) and also can penetrate the active site of the protein. The minimum binding free energy of the docked structure of **complex (1), complex (2)**, **complex (3)**, **complex (4)**, **complex (5), Crizotinib,** and **niclosamide** was obtained -88.898, -84.707, -86.298, -88.546, -100.203, -81.372 and -89.021 kcal/mol, respectively. All five Cu(II) complexes have shown better performance than the **Crizotinib** drug with the lowest binding free energy (-88.898, -84.707, -86.298, -88.546 and -100.203 kcal/mol, respectively). The planar structure of these compounds has caused more amino acids to be placed in the active cavity. These findings strongly suggested that inhibition of STAT3 signaling by **complex 5** may serve as an effective approach for colon treatment as compared with other complexes due to higher negative values, **Crizotinib**, and **niclosamide**. Also, in the section on HOMO and LUMO computational chemistry studies, we showed that **complex 5** acts as a soft molecule compared to other complexes, and this difference can be due to the variety of interactions in the structure of these compounds. As well as, a

better result was observed in the docking section than in other complexes. As shown in **Fig. 6**, the interaction between all complexes and proteins included Alkyl and Pi-Alkyl. All interactions are given in **Table 5**.

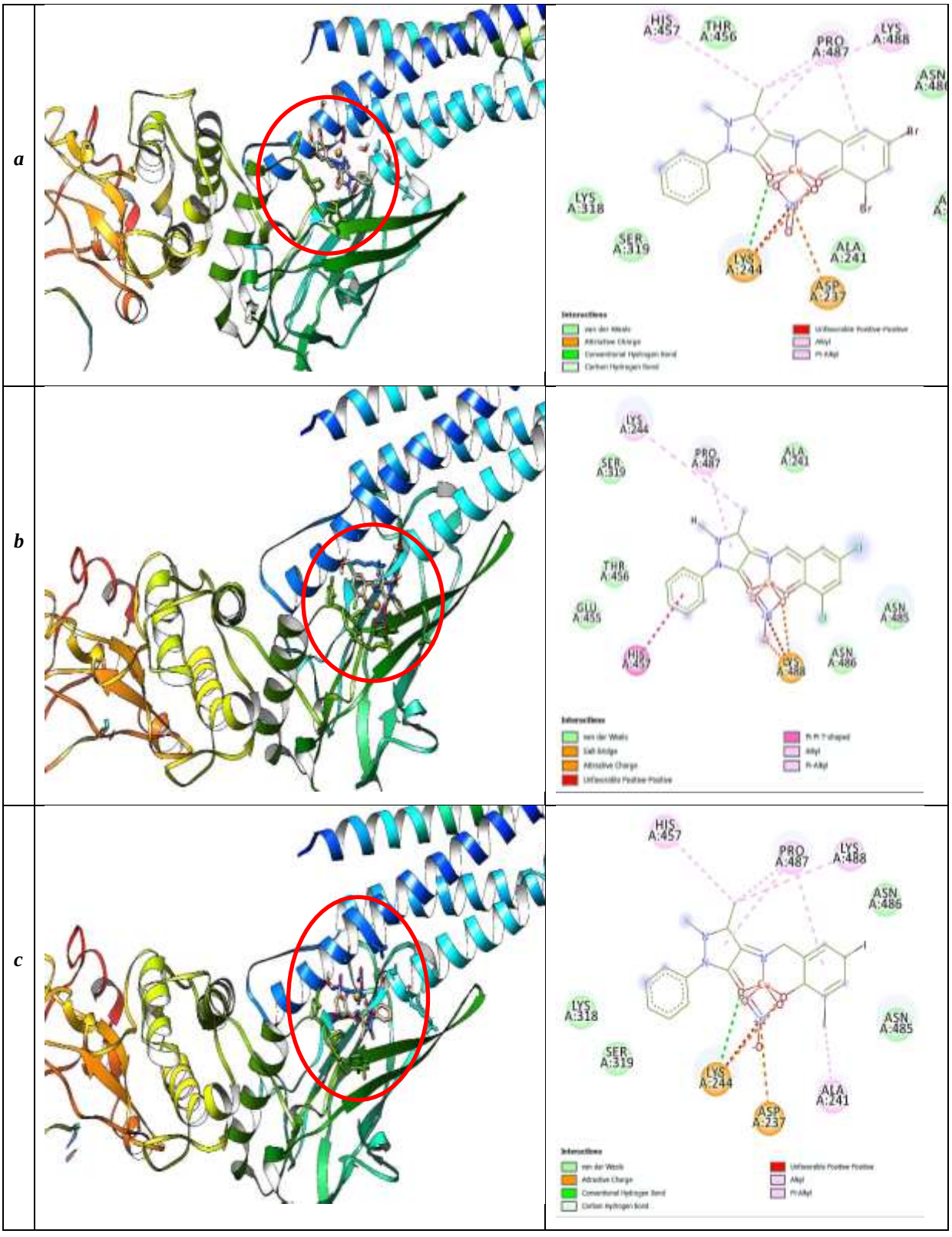

d		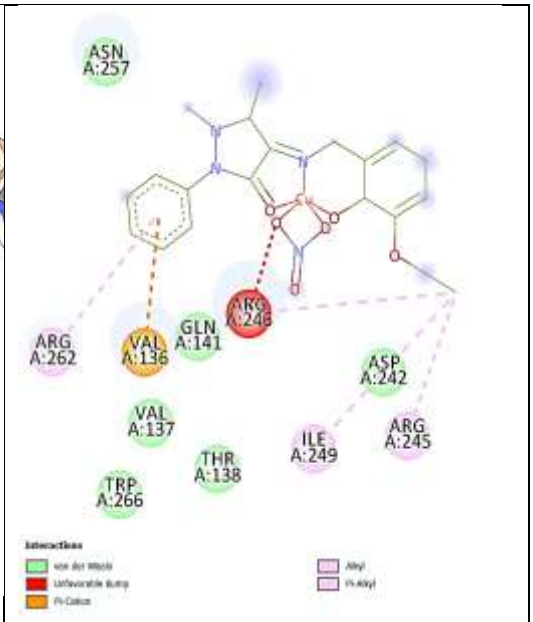 ASN A:257 ARG A:262 VAL A:136 GLN A:141 ARG A:248 ASP A:242 VAL A:137 ILE A:249 ARG A:245 THR A:138 TRP A:266
e	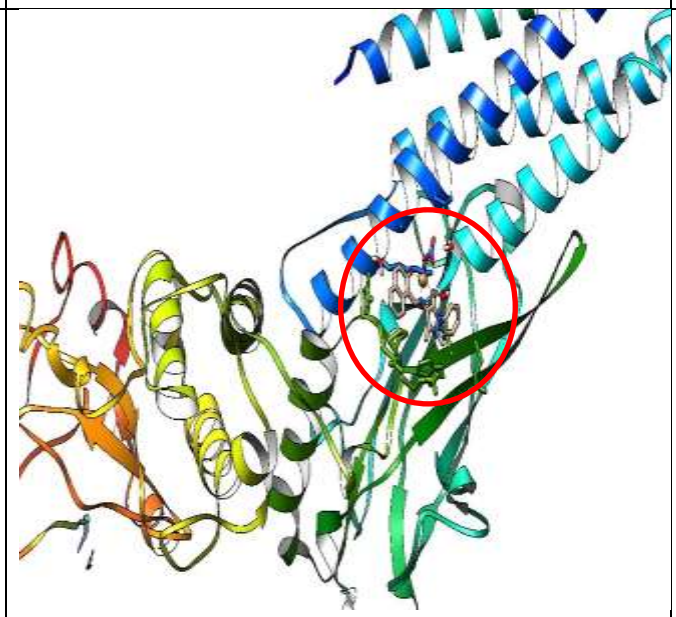	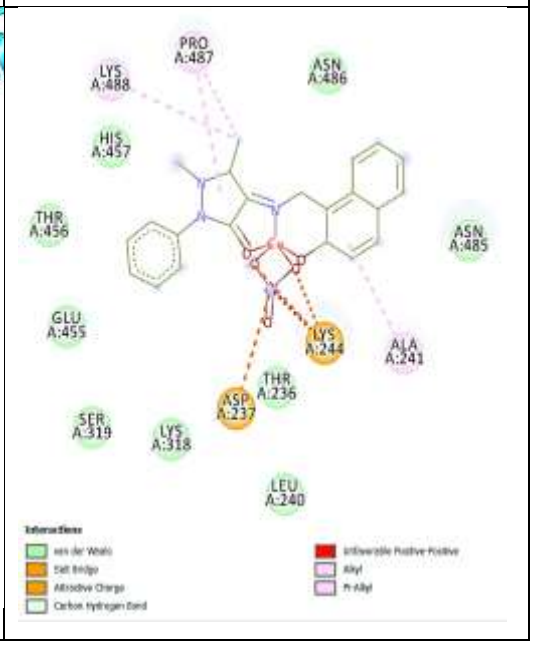 PRO A:487 LYS A:488 ASN A:486 HIS A:457 THR A:456 ASN A:485 GLU A:455 LYS A:244 ALA A:241 THR A:236 ASP A:237 SER A:319 LYS A:318 LEU A:240

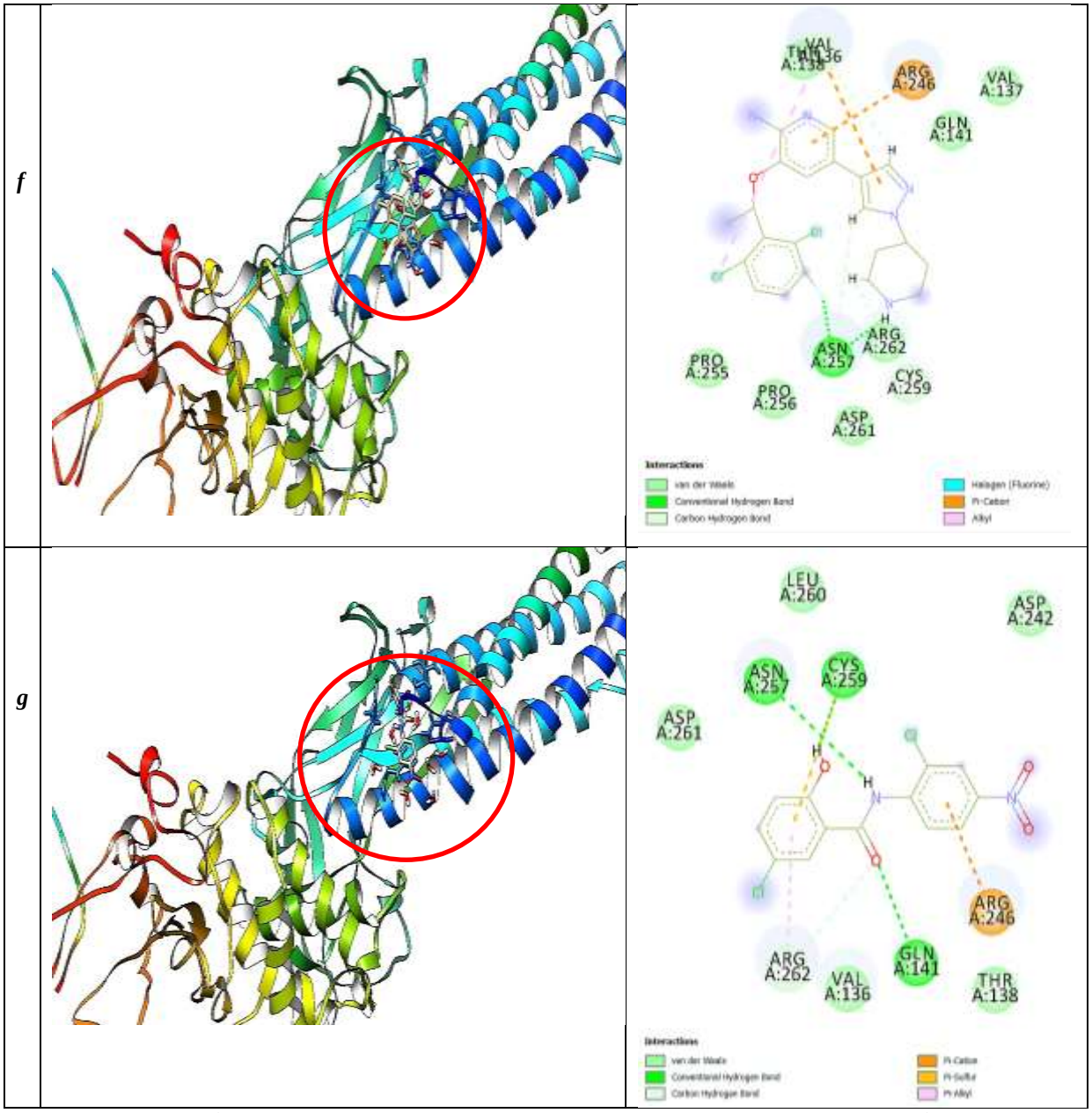

Figs 6. The interaction of (a); complex **(1)**, (b); complex **(2)**, (c); complex **(3)**, (d); complex **(4)**, and (e); complex **(5)**, (f); Crizotinib, and (g); Niclosamide with 1bg1.

Table 5. Bases of protein obtained from docking calculations with complexes.

compounds	Van der Waals	Carbon hydrogen bond	Hydrogen bond	Alkyl and Pi-Alkyl	Pi-Pi T-shaped
complex 1	Lys A:318, Ser A:319, Asn A:486, Asn A:485, Ala A:241	Pro A:487	Thr A:456	His A:457, Pro A:487, Lys A:488	
complex 2	Asn A:486, Asn A:485, Ala A:241, Ser A:319, Thr A:456			Lys A:244, Pro A:487,	His A:457
complex 3	Asn A:486, Lys A:318, Ser A:319,	Asn A:486		His A:457, Pro A:487, Lys A:488, Ala A:241	
complex 4	Asn A:257, Gln A:141, Val A:137, Trp A:266, Thr A:138, Asp A:242			Arg A:262, Ile A:249, Arg A:245	
complex 5	His A:457, Thr A:456, Glu A:455, Ser A:319, Lys A:318, Thr A:236, Leu A:240, Asn A:485, Asn A:486			Lys A:488, Pro A:487, Ala A:241	
Crizotinib	Thr A:138, Val A:136, Arg A:262, Asp A:261, Pro A:256, Pro A:255	Cys A:259,	Asn A:257,		

niclosamide	Leu A:260, Asp A:242, Asp A:261, Val A:136, Thr A:138	Arg A:262,	Asn A:257, Cys A:259, Glun A:141

4 -Conclusion

Five novel Cu(II) complexes were prepared from pyrazolone derivatives and identifications by elemental analysis, FT-IR, UV-Vis spectroscopy, and cyclic voltammetry (CV). All structure complexes were investigated by DFT, MEP, and QTAIM theoretical studies. Computational results of FT-IR and UV-Vis spectra theoretical studies are consistent with experimental results. Theoretical calculations, including DFT and molecular docking, provided insights into the electronic and structural properties of Cu(II) complexes. These calculations highlighted the compound's stability and reactivity, suggesting its potential as an anti-cancer agent. **Complex** (**2**) was calculated with greater stability and greater hardness with a higher HOMO-LUMO energy gap compared to other complexes. The theory of QTAIM suggests M-O/M-N interactions a non-covalent of ionic nature. Cu(II) complexes were studied for molecular docking to discover new drugs and the tendency to inhibit the cancer target protein STAT3 (1bg1). All complexes can effectively interact with the cancer molecular target protein STAT3 (1bg1) and have negative binding free energy. Also, all Pyrazolone compounds showed better performance than **crizotinib**. Among the Cu(II) complexes, **complex (5)** is expected to inhibit STAT3 signaling better with a higher negative value, as an effective approach for colon treatment compared to **crizotinib** and **niclosamide**.

Acknowledgments

We thank Semnan University for supporting this study. This research is supported by the Postdoc grant of the Semnan University (number 23336).

Institutional Review Board Statement

Not applicable.

Informed Consent Statement

Not applicable.

Conflicts of Interest

The authors declare no conflict of interest.

Appendixes

Appendixes appear after Conflicts of Interest.

Availability of data and materials

All data generated or analyzed during this study are included in this published article. Data available in article supplementary material, the data that supports the findings of this study are available in the supplementary material of this article.

Reference

[1] Karrouchi, K., Radi, S., Ramli, Y., Taoufik, J., Mabkhot, Y. N., Al-Aizari, F. A., & Ansar, M. H., (2018). Synthesis and Pharmacological Activities of Pyrazole Derivatives: A Review. *Molecules.*, 23(1), 134.

[2] Ghasemi, L., Behzad, M., Gharib, A., Arab, A., & Abbasi, A., (2023). A pyrazolone-based dinuclear Cu(II) Schiff-base complex: DFT studies on the rate-determining steps of the tautomerism in the ligand and molecular docking modelling with COVID-19 main protease (6LU7). *J. Coord. Chem*., 76(5-6), 830-846.

[3] Raman, N., Johnson Raja, S., & Sakthivel, A., (2009). Transition metal complexes with Schiff-base ligands: 4-aminoantipyrine based derivatives–a review. *J. Coord. Chem*., 62(5), 691-709.

[4] Poormohammadi, E. B., Behzad, M., Abbasi, Z., & Astaneh, S. D. A., (2020). Copper complexes of pyrazolone-based Schiff base ligands: Synthesis, crystal structures and

antibacterial properties. *J. Mol. Struct*., 1205,127603.

[5] Yadav, P., Kumari, M., Jain, Y., Agarwal, M., & Gupta, R., (2020). Antipyrine based Schiff's base as a reversible fluorescence turn "off-on-off" chemosensor for sequential recognition of Al^{3+} and F^{-} ions: A theoretical and experimental perspective. *Spectrochim. Acta A Mol. Biomol. Spectrosc*., 227, 117596.

[6] Mandal, S., Mondal, M., Biswas, J. K., Cordes, D. B., Slawin, A. M., Butcher, R. J., Saha, M., & Saha, N. C., (2018). Synthesis, characterization and antimicrobial activity of some nickel, cadmium and mercury complexes of 5-methyl pyrazole-3yl-N-(2′-methylthiophenyl) methyleneimine, (MPzOATA) ligand. *J. Mol. Struct*., 1152, 189-198.

[7] Wang, W. Jin, L., & Yu, Z., (2012). A Highly Active Ruthenium(II) Pyrazolyl–Pyridyl–Pyrazole Complex Catalyst for Transfer Hydrogenation of Ketones. *Organometallics*., 31(15), 5664-5667.

[8] Haiduc, I., (2019). ReviewInverse coordination. Organic nitrogen heterocycles as coordination centers. A survey of molecular topologies and systematization. Part 1. Five-membered and smaller rings. *J. Coord. Chem*., 72(13), 2127-2159.

[9] Matada, M. N., & Jathi, K., (2019). Pyrazole-based azo-metal(II) complexes as potential bioactive agents: synthesis, characterization, antimicrobial, anti-tuberculosis, and DNA interaction studies. *J. Coord. Chem*., 72(12), 1994-2014.

[10] Mandal, S., Das, M., Das, P., Samanta, A., Butcher, R. J., Saha, M., Alswaidan, I. A., L., Rhyman, Ramasami, P., & Saha, N. C., (2019). Synthesis, characterization, DFT and antimicrobial studies of transition metal ion complexes of a new schiff base ligand, 5-methylpyrazole-3yl-N-(2́-hydroxy phenyl amine) methyleneimine, (MPzOAP). *J. Mol. Struct.*, 1178, 100-111.

[11] Marchetti, F., Pettinari, C., Di Nicola, C., Tombesi, A., & Pettinari, R., (2019). Coordination chemistry of pyrazolone-based ligands and applications of their metal complexes. *Coord. Chem. Rev.*, 401, 213069.

[12] Marchetti, F., Pettinari, C., & Pettinari, R., (2005). Acylpyrazolone ligands: Synthesis, structures, metal coordination chemistry and applications. *Coord. Chem. Rev*., 249 (24), 2909–2945.

[13] Casas, J. S., Garcia-Tasende, M. S., Sanchez, A., Sordo, J., & Touceda, A., (2007). Coordination modes of 5-pyrazolones: A solid-state overview. *Coord. Chem. Rev*., 251, 1561-1589.

[14] Marchetti, F., Pettinari, R., & Pettinari, C., (2015). Recent advances in acylpyrazolone metal complexes and their potential applications. *Coord. Chem. Rev*., 303, 1–31.

[15] Berhanu, A.L., Mohiuddin, I., Malik, A.K., Aulakh, J.S., Kumar, V. & Kim, K.H., (2019). A review of the applications of Schiff bases as optical chemical sensors. *TrAc Trend. Anal. Chem*., 116, 74-91.

[16] Antony, R., Arun, T., & Manickam S. T. D., (2019). A review on applications of chitosan-based Schiff bases. *Int. J. Biol. Macromol*.,129, 615-633.

[17] Zhang, J., Xu, L. & Wong, W.Y., (2018). Energy materials based on metal Schiff base complexes. *Coord. Chem. Rev*., 355, 180-198.

[18] Liu, X., Manzur, C., Novoa, N., Celedón, S., Carrillo, D. & Hamon, J.R., (2018). Multidentate unsymmetrically-substituted Schiff bases and their metal complexes: Synthesis, functional materials properties, and applications to catalysis. *Coord. Chem. Rev*., 357, 144-172.

[19] Kaczmarek, M.T., Zabiszak, M., Nowak, M. & Jastrzab, R., (2018). Lanthanides: Schiff base complexes, applications in cancer diagnosis, therapy, and antibacterial activity . *Coord. Chem. Rev*., 370, 42-54.

[20] Iscen, A., Brue, C.R., Roberts, K.F., Kim, J., Schatz, G.C. & Meade, T.J., (2019). Inhibition of Amyloid-β Aggregation by Cobalt(III) Schiff Base Complexes: A Computational and Experimental Approach. *J. Am. Chem. Soc*. 141, 16685-16695.

[21] Siegel, R.L., Miller, K.D. & Jemal, A., (2015). Cancer statistics, 2015. *Statistics CA: Cancer J. Clin.*, 65(1), 5-29.

[22] Czarnomysy, R., Surażyński, A., Muszynska, A., Gornowicz, A., Bielawska, A. & Bielawski, K., (2018). A novel series of pyrazole-platinum(II) complexes as potential anti-cancer agents that induce cell cycle arrest and apoptosis in breast cancer cells. *J. Enzym. Inhib. Med. Chem*., 33, 1006-1023.

[23] Kachalaki, S., Ebrahimi, M., Khosroshahi, L.M., Mohammadinejad, S. & Baradaran, B., (2016). Cancer chemoresistance; biochemical and molecular aspects: a brief overview. *Eur. J. Pharmaceut. Sci*., 89, 20-30.

[24] Palanimurugan, A., & Kulandaisamy A., (2018). DNA, in vitro antimicrobial/anticancer activities and biocidal based statistical analysis of Schiff base metal complexes derived from salicylalidene-4-imino-2,3-dimethyl-1-phenyl-3-pyrazolin-5-one and 2-aminothiazole. *J. Organomet. Chem.*, 861, 263-274.

[25] Palanimurugan, A., Dhanalakshmi, A., Selvapandian, P., & Kulandaisamy A., (2019). Electrochemical behavior, structural, morphological, Calf Thymus-DNA interaction and in-vitro antimicrobial studies of synthesized Schiff base transition metal complexes. *Heliyon*, 5(7), e02039.

[26] Hussain, A., AlAjmi, M.F., Rehman, M.T., Amir, S., Husain, F.M., Alsalme, A., Siddiqui, M.A., AlKhedhairy, A.A. & Khan, R.A., (2019). Copper(II) complexes as potential anticancer and Nonsteroidal anti-inflammatory agents: In vitro and in vivo studies. *Sci. Rep*. 9, 5237.

[27] a) Matada, M.N. & Jathi, K., (2019). Pyrazole-based azo-metal(II) complexes as potential bioactive agents: synthesis, characterization, antimicrobial, anti-tuberculosis, and DNA interaction studies. *J. Coord. Chem*., 72 (12), 1994-2014. b) Kumar, V., El-Massaoudi, M., Radi, S., Van Hecke, K., Rotaru, A. & Garcia, Y., (2020). Iron(ii) coordination pyrazole complexes with aromatic sulfonate ligands: the role of ether. *New J. Chem*., 44(32),13902-13912.

[28] Kacar, S., Unver, H., & Sahinturk, V., (2020). A mononuclear copper(II) complex containing benzimidazole and pyridyl ligands: Synthesis, characterization, and

antiproliferative activity against human cancer cells. *Arabian. J. Chem*., 13(2), 4310-4323.

[29] Sakai, K., Tomita, Y., Ue, T., Goshima, K., Ohminato, M., Tsubomura, T., Matsumoto, K., Ohmura, K., & Kawakami, K., (2000). Syntheses, antitumor activity, and molecular mechanics studies of cis-$PtCl_2(pzH)_2$ (pzH=pyrazole) and related complexes. Crystal structure of a novel Magnus-type double-salt $[Pt(pzH)_4]$ $[PtCl_4][cis\text{-}PtCl_2(pzH)_2]_2$ involving two perpendicularly aligned 1D chains. *Inorg. Chim. Acta*., 297, 64-71.

[30] Aljuhani, E., Aljohani, M.M., Alsoliemy, A., Shah, R., Abumelha, H.M., Saad, F.A., Hossan, A., Al-Ahmed, Z.A., Alharbi, A., & El-Metwaly, N.M., (2021). Synthesis and characterization of Cu(II)-pyrazole complexes for possible anticancer agents; conformational studies as well as compatible in-silico and in-vitro assays. *Heliyon*, 7(11), e08485.

[31] Ali, P., Meshram, J., Sheikh, J., Tiwari, V., Dongre, R., & Hadda, T.B., (2012). Predictions and correlations of structure activity relationship of some aminoantipyrine derivatives on the basis of theoretical and experimental ground. *Med. Chem. Res*., 21, 157-164.

[32] Layek, S., Ganguly, R., & Pathak, D. D., (2018). Unprecedented formation of a μ-oxobridged polymeric copper(II) complex: Evaluation of catalytic activity in synthesis of 5-substituted 1H-tetrazoles. *J. Org. Chem.*, 870, 16-22.

[33] Selvakumar, P. M., Suresh, E., & Subramanian, P. S., (2007). Synthesis, spectral characterization and structural investigation on some 4-aminoantipyrine containing Schiff base Cu(II) complexes and their molecular association. *Polyhedron*, 26(4), 749-756.

[34] Medzhidov, A. A., Fatullaeva, P. A., Peng, S. M., Ismaiylov, R. G., Lee, G. H., & Garaeva, S. R., (2012). Oxidative dehydrogenation of N-(2-hydroxy-3,5-R1, R2-benzyl)-4-aminoantipyrines in the complexation reaction. *Russ. J. Coord. Chem*., 38, 126-133.

[35] Raman, N., Johnson Raja, S., & Sakthivel, A., (2009). Transition metal complexes with Schiff-base ligands: 4-aminoantipyrine based derivatives–a review. *J. Coord. Chem*, 62(5), 691-709.

[36] Liu, Z.C., Yang, Z.Y., Li, T.R., Wang, B.D., Li, Y., & Wang, M.F., (2011). DNA-binding, antioxidant activity and solid-state fluorescence studies of copper(II), zinc(II) and nickel(II) complexes with a Schiff base derived from 2-oxo-quinoline-3-carbaldehyde. *Transition Met Chem.*, 36, 489-498.

[37] Fatullayeva, P. A., Medjidov, A. A., Maharramov, A. M., Gurbanov, A. V., Askerov, R. K., Rahimov, K. Q., Kopylovich, M. N., Mahmudov, K. T., & Pombeiro A. J., (2012). New cobalt(II) and nickel(II) complexes of 2-hydroxy-benzyl derivatives of 4-aminoantipyrine. *Polyhedron*, 44(1), 72-76.

[38] Parvarinezhad, S., Salehi, M., Kubicki, M., & Khaleghian A., (2021). Unprecedented formation of a μ-oxobridged dimeric copper (II) complex: Evaluation of structural, spectroscopic, and electronic properties by using theoretical studies and investigations biological activity studies of new Schiff bases derived from pyrazolone. *Appl. Organomet. Chem*., 35(12), e6443.

[39] Parvarinezhad, S., Salehi, Kubicki, M., & Eshaghi Malekshah, R., (2022). Synthesis, characterization, spectral studies and evaluation of noncovalent interactions in co-crystal of μ-oxobridged polymeric copper(II) complex derived from pyrazolone by theoretical studies. *J. Mol. Struct.*, 1260,132780.

[40] Parvarinezhad, S., Salehi, M., Eshaghi Malekshah, R., Kubicki, M., & Khaleghian, A., (2022). Synthesis, characterization, spectral studies two new transition metal complexes derived from pyrazolone by theoretical studies, and investigate anti-proliferative activity. *Appl. Organomet. Chem*., 36(3), e6563.

[41] Huang, L., & Chen, D.B., (2005). link to html4-{[(1E)- (3,5-Dibromo-2 hydroxy-phen-yl) methyl-ene] -amino}-1,5-dimethyl-2-phenyl-1,2-dihydro-3H-pyrazol-3-one. *Act Crystallogr, E*., 61(12), o4169-o4170.

[42] Selvakumar, P.M., Suresh, E., & Subramanian, P.S., (2007). Synthesis, spectral characterization and structural investigation on some 4-aminoantipyrine containing Schiff base Cu(II) complexes and their molecular association. *Polyhedron*., 26(4), 749-756.

[43] Zhang, X., (2011). Syntheses, Crystal Structures and Antibacterial Activities of Two Antipyrine Derivatives. *J. Chem. Crystallogr*, 41(7), 1044-1048.

[44] Mohamed, S.K., Mague, J.T., Akkurt, M., Albayati, M.R., & Mohamed, A.F., (2017). 4-{(E)-[(2-Hy-dr-oxy-naphthalen-1-yl) methyl-idene] amino}-1,5-di-methyl-2-phenyl-2,3-di-hydro-1H-pyrazol-3-one: a new polymorph (β-phase). IUCrData., 2(8), x171166.

[45] Ouennoughi, Y., Eddine Karce, H., Aggoun, D., Lanez, T., Ruiz-Rosas, R., Bouzerafa, B., Ourari, A., Morallon, E., (2017). A novel ferrocenic copper(II) complex Salen-like, derived from 5-chloromethyl-2-hydroxyacetophenone and N ferrocenmethylaniline: Design, spectral approach and solvent effect towards electrochemical behavior of Fc^{+}/Fc redox couple, *J. Organ. Chem.*, 848, 344-351.

[46] Deilami, A.B., Salehi, M., Arab, A. & Amiri, A., (2018). Synthesis, crystal structure, electrochemical properties and DFT calculations of three new Zn(II), Ni(II) and Co(III) complexes based on 5-bromo-2-((allylimino)methyl) phenol Schiff-based ligand. *Inorganica Chim. Acta*, 476, 93-100.

[47] Frisch, M.J., Trucks, G.W., Schlegel, H.B., Scuseria, G.E., Robb, M.A., Cheeseman, J.R., Montgomery Jr, J.A., Vreven, T., Kudin, K.N., Burant, J.C., Millam, J.M., Iyengar, S.S., Tomasi, J., Barone, V., et al., (2009), Gaussian 09 (Linux version).

[48] El-Ayaan, U., El-Metwally, N.M., Youssef, M.M., & El Bialy, S.A., (2007). Perchlorate mixed–ligand copper(II) complexes of β-diketone and ethylene diamine derivatives: Thermal, spectroscopic and biochemical studies. *Spectrochim. Acta A*., 68, 1278-1286.

[49] Ray, R.K., & Kauffman, G.R., (1990). EPR Spectra and covalency of bis(amidinourea/O-alkyl-1-amidinourea) copper (II) complexes Part II. Properties of the CuN42− chromophore. *Inorg. Chim. Acta*., 173, 207-214.

[50] Mashat, K.H., Babgi, B.A., Hussien, M.A., Arshad, M.N., & Abdellattif, M.H., (2019). Synthesis, structures, DNA-binding and anticancer activities of some copper(I)-phosphine complexes. *Polyhedron*, 158, 164-172.

[51] Parvarinezhad, S., Salehi, M., Kubicki, M., & Malekshah, R. E., (2022). Experimental and theoretical studies of new Co(III) complexes of hydrazide derivatives proposed as multi-target inhibitors of SARS-CoV-2. *Appl. Organomet. Chem*., 36(10), e6836.

[52] Gholivand, K., Barzegari, A., Yousefian, M., Malekshah, R.E., & Faraghi, M., (2023). Experimental and theoretical evaluation of biological properties of a phosphoramide functionalized graphene oxide *Biocatal. Agric. Biotechnol*, 47, 102612.

[53] Gholivand, K., Sabaghian, M., & Malekshah, R. E., (2021). Synthesis, characterization, cytotoxicity studies, theoretical approach of adsorptive removal and molecular calculations of four new phosphoramide derivatives and related graphene oxide. *Bioorg. Chem.*, 115, 105193.

[54] Ramezanipoor, S., Parvarinezhad, S., Salehi, M., Grześkiewicz, A. M., & Kubicki, M., (2022). Crystal structures, electrochemical properties and theoretical studies of three New Zn(II), Mn(III) and Co(III) Schiff base complexes derived from 2-hydroxy-1-allyliminomethyl-naphthalen. *J. Mol. Struct.*, 1257, 132541.

[55] Sepehrfar, S., Salehi, M., Parvarinezhad, S., Grześkiewicz, A.M., & Kubicki, M., (2023). New Cu(II), Mn(II) and Mn(III) Schiff base complexes cause noncovalent interactions: X-ray crystallography survey, Hirshfeld surface analysis and molecular simulation investigation against SARS-CoV-2. *J. Mol. Struct.*, 1278, 134857.

[56] Saad, F.A., Elghalban, M.G., El-Metwaly, N.M., El-Ghamry, H., & Khedr, A.M., (2017). Density functional theory/B3LYP study of nanometric 4-(2,4-dihydroxy-5-formylphen-1-ylazo)-N-(4-methylpyrimidin-2-yl) benzene sulfonamide complexes: Quantitative structure–activity relationship, docking, spectral and biological investigations. Appl. *Organomet. Chem*., 31, ec3721.

[57] Ali, P., Meshram, J., Sheikh, J., Tiwari, V., Dongre, R., & Hadda, T.B., (2012). Predictions and correlations of structure activity relationship of some aminoantipyrine derivatives on the basis of theoretical and experimental ground. *Med. Chem. Res*., 21, 157–164.

[58] Fatullayeva, P.A., Medjidov, A.A., Maharramov, A.M., Gurbanov, A.V., Askerov, R.K., Rahimov, K.Q., Kopylovich, M.N., Mahmudov, K.T., & Pombeiro, A.J., (2012). New cobalt(II) and nickel(II) complexes of 2-hydroxy-benzyl derivatives of 4-aminoantipyrine. *Polyhedron*., 44(1), 72-76.

[59] Loukopoulos, E., Berkoff, B., Abdul-Sada, A., Tizzard, G.J., Coles, S.J., Escuer, A., & Kostakis, G.E., (2015). A Disk-Like CoII3DyIII4 Coordination Cluster Exhibiting Single Molecule Magnet Behavior. *Eur. J. Inorg. Chem*., 2015, 2646– 2649.

[60] El-Sonbati, A.Z., El-Mogazy, M.A., Nozha, S.G., Diab, M.A., Abou-Dobara, M.I., Eldesoky, A.M., & Morgan, S.M., (2022). Mixed ligand transition metal(II) complexes:

Characterization, spectral, electrochemical studies, molecular docking and bacteriological application. *J. Mol. Struc*., 1248, 131498.

[61] El-Sonbati, A.Z., Diab, M.A., Morgan, S.M., Abou-Dobara, M.I., & El-Ghettany, A.A., (2020). Synthesis, characterization, theoretical and molecular docking studies of mixed-ligand complexes of Cu(II), Ni(II), Co(II), Mn(II), Cr(III), UO2(II) and Cd(II). *J. Mol. Struct*., 1200, 127065.

[62] El-Metwally, N.M., El-Shazly, R.M., Gabr, I.M., & El-Asmy, A.A., (2005). Physical and spectroscopic studies on novel vanadyl complexes of some substituted thiosemicarbazides. *Spectrochim. Acta A*, 61, 1113-1119.

[63] Lever, A.B.P., (1986). Inorganic Electronic Spectroscopy. *Elsevier, Amsterdam*.

[64] Selvakumar, P. M., Suresh, E., & Subramanian, P. S., (2007). Synthesis, spectral characterization and structural investigation on some 4-aminoantipyrine containing Schiff base Cu(II) complexes and their molecular association. *Polyhedron*, 26(4), 749-756.

[65] Hökelek, T., Kiliç, Z., ISIKLAN, M., & Hayvali, M., (2002). Crystal structure of 4-{[(1E)- (2-hydroxynaphthyl) methylidene] amino}-1, 5-di methyl-2-phenyl-2, 3-dihydro-1H-pyrazol-3-one. *Anal. Sci*., 18, 215-216.

[66] Zhou, Y.H., Liu, X.W., Chen, L.Q., Wang, S.Q., & Cheng, Y., (2016). Synthesis, structure and superoxide dismutase-like activity of two mixed-ligand Cu(II) complexes with N, N′-bis(2-pyridylmethyl) amantadine, *Polyhedron*., 117, 788-794.

[67] Mandal, S., Chatterjee, S., Modak, R., Sikdar, Y., Naskar, B., & Goswami, S., (2014). Syntheses, crystal structures, spectral studies, and DFT calculations of two new square planar Ni(II) complexes derived from pyridoxal-based Schiff base ligands. *J. Coord. Chem.*, 67(4), 699-713.

[68] Grabowski, S.J., (2011). What Is the Covalency of Hydrogen Bonding? Chem. Rev., 111(4), 2597-2625.

[69] Ruiz, A., Pérez, H., Morera-Boado, C., Almagro, L., da Silva, C.C., Ellena, J., de la Vega, J.M.G., Martínez-Álvarez, R., Suárez, M., & Martín, N., (2014). Unusual hydrogen bond patterns contributing to supramolecular assembly: conformational study, Hirshfeld surface analysis and density functional calculations of a new steroid derivative. CrystEngComm., 16(33), 7802-7814.

[70] Shi, L., Zheng, H., Hu, W., Zhou, B., Dai, X., Zhang, Y., Liu, Z., Wu, X., Zhao, C., & Liang, G., (2017). Niclosamide inhibition of STAT3 synergizes with erlotinib in human colon cancer. Onco Targets Ther., 10,1767-1776.